Research Institute for Advanced Computer Science
NASA Ames Research Center

An Edge-Based Solution-Adaptive Method Applied to the AIRPLANE Code

Rupak Biswas
Scott D. Thomas
Susan E. Cliff

RIACS Technical Report 95.22 November 1995

Paper No. AIAA-96-0553, presented at the *AIAA 34th Aerospace Sciences Meeting & Exhibit*, Reno, Nevada, January 15–18, 1996

An Edge-Based Solution-Adaptive Method Applied to the AIRPLANE Code

Rupak Biswas
Scott D. Thomas
Susan E. Cliff

The Research Institute of Advanced Computer Science is operated by Universities Space Research Association, The American City Building, Suite 212, Columbia, MD 21044, (410) 730-2656

Work reported herein was supported by NASA via Contract NAS 2-13721 between NASA and the Universities Space Research Association (USRA). Work was performed at the Research Institute for Advanced Computer Science (RIACS), NASA Ames Research Center, Moffett Field, CA 94035-1000.

AN EDGE-BASED SOLUTION-ADAPTIVE METHOD APPLIED TO THE AIRPLANE CODE*

Rupak Biswas†
RIACS, NASA Ames Research Center, Moffett Field, CA

S25277245

Scott D. Thomas‡
Sterling Software Inc., 1121 San Antonio Road, Palo Alto, CA

Susan E. Cliff§
High Speed Aerodynamics Branch, NASA Ames Research Center, Moffett Field, CA

ABSTRACT

Computational methods to solve large-scale realistic problems in fluid flow can be made more efficient and cost effective by using them in conjunction with dynamic mesh adaption procedures that perform simultaneous coarsening and refinement to capture flow features of interest. This work couples the tetrahedral mesh adaption scheme, called 3D_TAG, with the AIRPLANE code to solve complete aircraft configuration problems in transonic and supersonic flow regimes. Results indicate that the near-field sonic boom pressure signature of a cone-cylinder is improved, the oblique and normal shocks are better resolved on a transonic wing, and the bow shock ahead of an unstarted inlet is better defined.

INTRODUCTION

Traditional computational methods can be made more efficient and cost effective by redistributing the available mesh points to capture flowfield phenomena of interest. Such adaptive procedures evolve with the solution and provide a robust and reliable methodology. Highly localized regions of mesh refinement are required in order to accurately capture shock waves, contact discontinuities, and shear layers. This provides the aerodynamicist with the opportunity to obtain flow solutions on adapted meshes that are comparable to those obtained on globally-fine grids.

Two types of solution-adaptive grid strategies are commonly used with unstructured-grid methods. Grid regeneration schemes generate a new grid with a higher or lower concentration of points in regions that are targeted by some error indicator. A major disadvantage of such schemes is that they are computationally expensive. This is a serious drawback for unsteady problems where the mesh must be frequently adapted. However, resulting grids are usually well-formed with smooth transitions between regions of coarse and fine mesh spacing.

Local mesh adaption, on the other hand, involves adding points to the existing grid in regions where the error indicator is high, and removing points from regions where the indicator is low. The advantage of such strategies is that relatively few mesh points need to be added or deleted at each adaptive step for unsteady problems. However, complicated logic and data structures are required to keep track of the points that are added and removed. Furthermore, the resulting grids can often have non-smooth transitions between coarse and fine mesh regions and a criterion for maintaining a level of grid quality is usually required.

This work couples the dynamic tetrahedral mesh adaption scheme,[1] called 3D_TAG, with the AIRPLANE code[2,3] to solve complete airplane configuration problems in transonic and supersonic flow regimes. The objective is to demonstrate the effectiveness of the local mesh adaption method to obtain improved solutions.

3D_TAG has been previously combined with TRI3D,[4] a finite volume upwind Euler code, to successfully model large problems in helicopter aerodynamics and aeroacoustics.[5,6] Results have demonstrated that appropriate error indicators can efficiently capture surface shocks, propagate acoustic signals with minimal dissipation, and accurately convect rotorcraft vortical wakes.

†Scientist, Member AIAA.

‡Software Specialist, Senior Member AIAA.

§Aerospace Engineer, Member AIAA.

The remainder of this report is divided into five sections. The first section briefly describes the AIRPLANE code. The next section describes the 3D_TAG tetrahedral adaption procedure. The third section highlights the modifications that were necessary in order to interface the two codes. Results obtained for a supersonic cone-cylinder, a transonic wing, and a supersonic inlet unstart problem are reported in the fourth section. Finally, we conclude by summarizing our observations from this work.

EULER FLOW SOLVER

AIRPLANE consists of two separate codes: FLOPLANE and MESHPLANE — the Euler flow solver and the grid generator, respectively. These programs were developed by Jameson and Baker to model complex configurations using unstructured grids. FLOPLANE[3] uses a finite-volume algorithm that computes flow variables at the vertices of a tetrahedral mesh. MESHPLANE[7,8] generates the tetrahedral elements by using a constrained Delaunay triangulation algorithm. The often complicated and time-consuming procedure of blocking and gridding structured multi-zone grids is eliminated by AIRPLANE, but some control over the distribution of mesh points is lost in the process.

In order to improve the turn-around time and computational efficiency, a parallel version of AIRPLANE has been recently established on the IBM SP2.[9] Results show that almost perfect scalability is obtained for up to 64 processors. This parallel version of AIRPLANE is used for the calculations in this report.

TETRAHEDRAL ADAPTION SCHEME

3D_TAG has its data structure based on edges that connect the vertices of a tetrahedral mesh. This means that each tetrahedral element is defined by its six edges rather than by its four vertices. This edge data structure makes the mesh adaption procedure capable of performing anisotropic refinement and coarsening. A successful data structure must contain only the information required to rapidly reconstruct the mesh connectivity when vertices are added or deleted while having a reasonable memory requirement.

At each mesh adaption step, individual edges are marked for coarsening, refinement, or no change. Only three subdivision types are allowed for each tetrahedral element and these are shown in Fig. 1. The 1:8 isotropic subdivision is implemented by adding a new vertex at the mid-point of each of the six edges. The 1:4 and 1:2 subdivisions can result either because the edges of a parent tetrahedron are targeted anisotropically or because they are required to form a valid connectivity for the new mesh. When an edge is bisected, the solution vector is linearly interpolated at the mid-point from the two points that constitute the original edge.

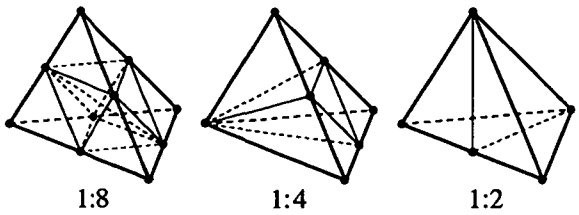

Figure 1: Three types of subdivision are permitted for a tetrahedral element.

Mesh refinement is performed by first setting a bit flag to one for each edge that is targeted for subdivision. The edge markings for each element are then combined to form a binary pattern as shown in Fig. 2 where the edges marked with an R are the ones to be bisected. Once this edge-marking is completed, each element is independently subdivided based on its binary pattern. Special data structures are used in order to ensure that this process is computationally efficient.

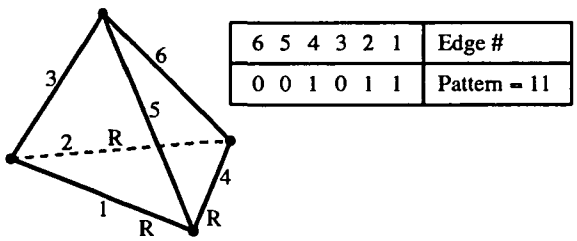

Figure 2: Sample edge-marking pattern for element subdivision.

Mesh coarsening also uses the edge-marking patterns. If a child element has any edge marked for coarsening, this element and its siblings are removed and their parent element is reinstated. The parent edges and elements are retained at each refinement step so they do not have to be reconstructed. Reinstated parent elements have their edge-marking patterns adjusted to reflect that some edges have been coarsened. The mesh refinement procedure is then invoked to generate a valid mesh.

A significant feature in 3D_TAG is the concept

of "sublists." A data structure is maintained where each vertex has a sublist of all the edges that are incident upon it. Also, each edge has a sublist of all the elements that share it. These sublists eliminate extensive searches and are crucial to the efficiency of the overall adaption scheme.

In the initial version of the code,[1] the data structure was implemented in C as a series of dynamically-allocated linked lists. This facilitated the addition and deletion of mesh points, but the linked lists made it very difficult to pass information directly to Fortran flow solvers. In order to reduce the communication overhead, the linked lists have been replaced with arrays and a garbage collection algorithm is used to compact free space when mesh points are removed.

An important component of any mesh adaption procedure is the choice of an error indicator for each region of the mesh. Typically, this error indicator is not a true estimate of the error in the solution; rather, it is an indicator of high gradients in the flowfield that are assumed to be regions of high error. Error indicators are usually problem-dependent and considerable fine tuning is often necessary to obtain satisfactory results.

COUPLING AIRPLANE AND 3D_TAG

The AIRPLANE and the 3D_TAG codes are currently loosely coupled. Relevant information is passed between the two programs via files. Historically, FLOPLANE expected the computational grid to be provided by MESHPLANE. With the inclusion of the mesh adaption procedure, the flow solver must also be able to read intermediate adapted meshes as well as read and write solution files generated by 3D_TAG. The input module of FLOPLANE has been modified to make this possible. 3D_TAG has also been customized to read and write mesh files that are in the format generated by MESHPLANE and expected by FLOPLANE.

Figure 3 shows how the three codes interact. MESHPLANE generates an initial unstructured tetrahedral grid based on input mesh parameters. This mesh is passed on to FLOPLANE which computes an acceptably converged solution. The initial mesh is also read by 3D_TAG that converts it to an edge-based representation and generates all the sublists.

When the first mesh refinement is desired, 3D_TAG is invoked and supplied with the initial converged solution. 3D_TAG generates a new mesh and interpolates the coarse-grid solution onto the new

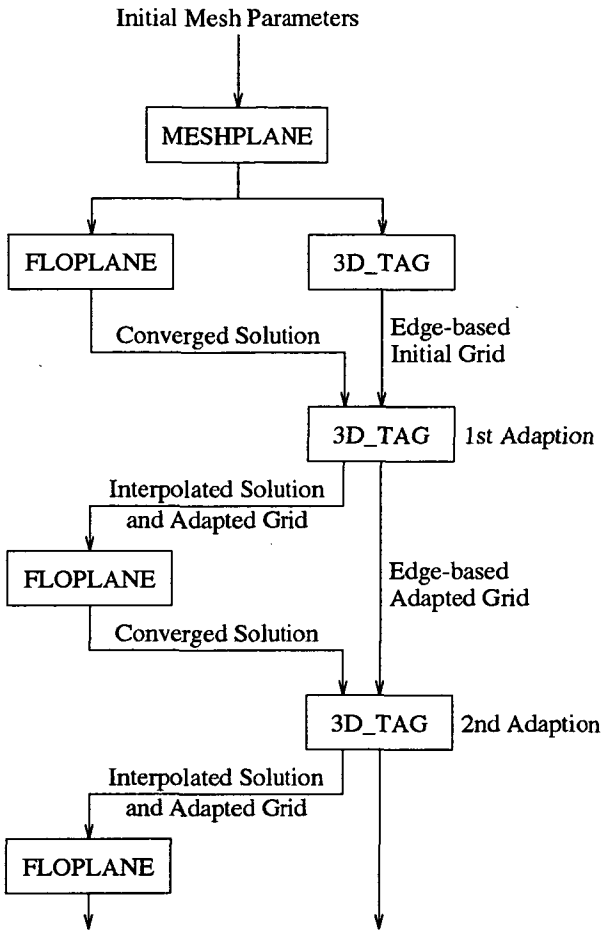

Figure 3: Interfacing AIRPLANE and 3D_TAG via files.

mesh. This mesh and the interpolated solution are given as input to FLOPLANE to further converge the solution. This entire process is then repeated if further mesh adaption steps are desired.

Note that at the end of each adaption step, 3D_TAG writes out its entire internal data structure to a file. This file not only contains all the mesh connectivity but also all information pertaining to the history of the mesh. The overhead of retaining storage for the parent elements and edges is typically small (less than 15% for the test cases in this report) but required to coarsen the mesh and/or to improve grid quality.[10]

The coupling strategy allows both AIRPLANE and 3D_TAG to remain modular and independent. However, because the interfacing is done through files, human intervention is required whenever the mesh has to be adapted. This is not a drawback for steady-flow problems where the mesh has to be

adapted only a few times and the user needs to visualize the grid and the solution before deciding how and where to adapt the mesh. Note that the entire procedure of repeatedly adapting the mesh and running the flow solver can be easily automated for problems with unsteady flows.

COMPUTATIONAL RESULTS

The coupled 3D_TAG and AIRPLANE codes were applied to a supersonic cone-cylinder, a transonic wing, and a supersonic inlet unstart problem. These examples were chosen as test cases that fully exercised all aspects of the mesh adaption scheme in three dimensions as well as demonstrated the range of problems that could be efficiently solved using the combined method.

The first test case involves computation of the near-field sonic boom pressure signature for a cone-cylinder. The cone-cylinder consists of three components: a cone of length $L = 8.6$ inches with a 6.48° included angle, a cylinder of length $2L$ extending downstream of the cone, and a second cone to close the cylinder to a point at a distance $4L$ from the nose. One-half of the configuration was modeled with AIRPLANE, since axisymmetric and quarter-plane modeling are not permitted. Flow conditions for this case were Mach 1.68 and an angle of attack of zero degrees.

A very coarse starting mesh was desired to rapidly assess the AIRPLANE-3D_TAG coupling with minimal computational resources. MESHPLANE was not used to generate the initial computational mesh because without modification to the algorithm, it is unable to generate extremely coarse meshes. MESHPLANE was developed to automatically generate meshes for complete aircraft. As a result, it generates grids of sufficient density near the surface to obtain reliable results.

The initial three-dimensional unstructured mesh for this case was created by subdividing a multi-block structured grid. Most hexahedra of a three-block C-H grid were subdivided into five tetrahedra. The near-, mid-, and far-field grid density of the three blocks decreased with distance from the model. The surface geometry was defined at 65 stations distributed uniformly from nose to tail. Circumferential cuts had 17 points, except the nose and tail were defined by a single point. The entire grid was swept at the free-stream Mach angle to reduce the number of mesh points. The upstream boundary was $0.5L$ ahead of the nose, while the downstream boundary was at least $6.7L$ aft of the tail. The upper, lower, and side boundaries were greater than $15L$ from the axis of the body.

The initial mesh consisted of 19,957 points, of which only 1073 were on the surface of the body. The small number of surface points led to faceting that was somewhat reduced by using the 3D_TAG code to geometrically refine the mesh within a neighborhood from the upstream boundary to the midpoint of the cylinder with radius 2.5 times that of the body.

The purpose of this test case is to predict the sonic boom pressure signature below the body and compare it with experimental data. The computational pressure signature was obtained at a distance L below the configuration ($h/L = 1$) in the symmetry plane and extrapolated to the experimental distance using the waveform parameter method of Thomas.[11] Since we are primarily interested in the weak finite-rise shock from the nose of the cone and the expansion waves from the cone-cylinder junction (shoulder), mesh refinement was restricted to a distance of $2L$ from the body in the radial direction and a distance $3L$ downstream of the nose, sheared at the free-stream Mach angle.

Table 1: Grid sizes through the adaption steps

	Vertices	Elements	Edges
Initial mesh	19,957	88,216	112,691
Geom. ref.	28,821	132,776	168,154
1st adapt.	71,785	367,522	451,924
2nd adapt.	129,722	703,396	848,171
3rd adapt.	212,251	1,187,366	1,415,967

A total of three solution-adaptive steps were performed. An error indicator based on pressure differences across edges was used to adapt the mesh. However, since acoustic pressure attenuates with distance from the source, the pressure difference across an edge was scaled by a function proportional to its distance from the body to obtain the error indicator. Converged solutions were obtained with 2000 FLOPLANE iterations after each refinement step. Table 1 presents the progression of grid sizes through the four adaption steps.

Figure 4 shows the sequence of meshes in the symmetry plane. The initial mesh as well as the adapted meshes after the three solution-adaptive steps are shown. Note that a coarsening phase removed some surface points on the cylindrical portion of the model where the pressure gradients are small or non-existant. Also, each refinement step was performed to maintain the same point density in the vicinity of the shock to at least a distance L from

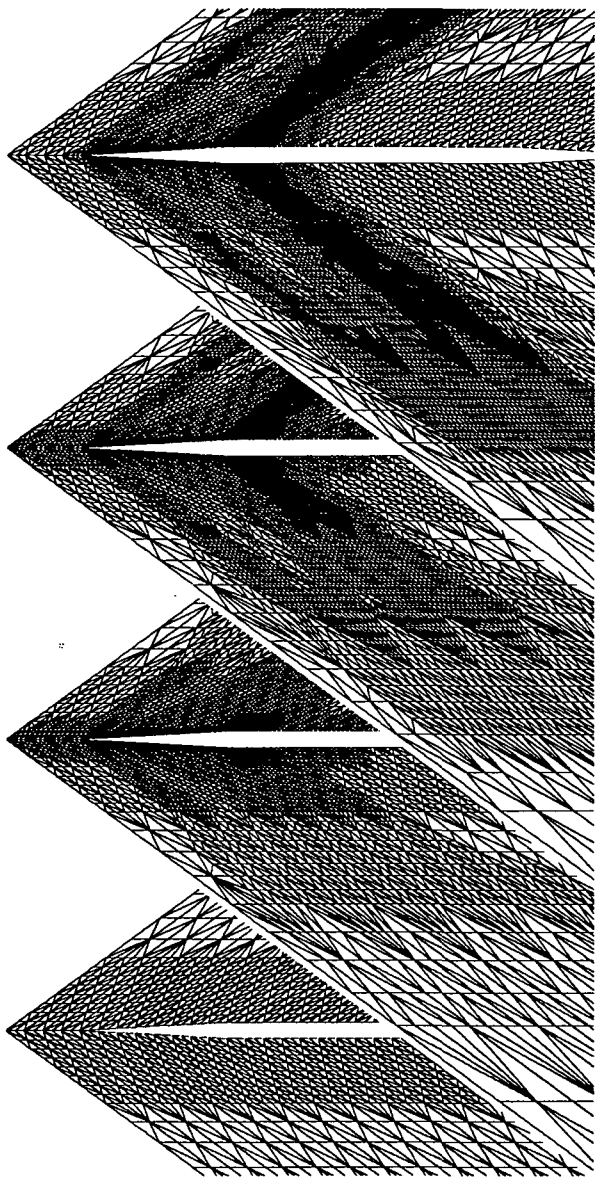

Figure 4: Several mesh adaption stages for the cone-cylinder, $M_\infty = 1.68$, $\alpha = 0.0°$.

the body where the pressure was sampled. A closeup of the final adapted mesh, shown in Fig. 5, confirms this. Horizontal lines are placed at the sampling location. Pressure contours are also depicted in Fig. 5. These contours show excellent resolution of the expansion waves at the shoulder.

The AIRPLANE and experimental pressure signatures are compared at an h/L of 10.0 in Fig. 6. Results are shown for both the initial coarse and the final adapted meshes. The computational data were taken at $h/L = 1.0$ and extrapolated to the experimental distance. For the sake of continuity, results are also shown from earlier work[12] where the computational data was extrapolated from an h/L of 0.1. The earlier computation underpredicts the finite-rise portion of the signature and the maximum overpressure. The new results on the final adapted mesh more accurately predict the finite-rise bow shock and maximum overpressure, but the expansion is slightly underpredicted in spite of the grid refinement around the shoulder. The pressure signatures for the adapted grid can be taken at larger distances from the model than for the non-adapted grid. This is significant since accurate signatures cannot be obtained at small sampling distances from typical non-axisymmetric configurations. The three-dimensional effects require a sampling distance of approximately half the span for reliable data. Finally, comparison with the coarse mesh results demonstrate the effectiveness of mesh adaption.

The second test case consists of a flow-field computation for the ONERA M6 wing[13] at Mach 0.84 and 3.06-degrees angle of attack . The model was an isolated, swept, tapered, untwisted wing mounted on a wind-tunnel wall. All wing sections are scaled from the 9.8%-thick symmetric root section. The tip chord is 0.562 and the half-span is 1.48, based on a root chord of unit length. The half-chord sweep of the wing is 23.2°. The primary challenge here is to accurately capture the lambda shock on the upper surface of the wing. The oblique shock near the leading edge is much weaker than the normal shock and is generally more difficult to resolve.

The initial three-dimensional computational mesh was created from a structured H-H mesh using a simple algebraic method. The outer boundaries were located approximately 15 root chords away from the wing in all directions. Each structured-grid hexahedron was then split into at most five tetrahedra. Collapsed hexahedra filling the wedge region beyond the flat tip yielded fewer than five tetrahedra each. Careful selection of diagonal edges at the blunt wing leading edge prevented the possibility of refined elements penetrating the surface.

The initial unstructured mesh consisted of 34,202 points, of which only 103 were on the wing surface. The small number of surface points led to severe faceting of the wing surface. Before a solution was attempted, this undesirable faceting was somewhat diminished by using the 3D_TAG code to geometrically refine the mesh within a box enclosing the M6 wing. This box extended one-half root chords fore and aft, above and below, and spanwise beyond the tip of the wing, and was swept with the leading and trailing edges. This refinement step increased the number of surface points to 378 and also reduced

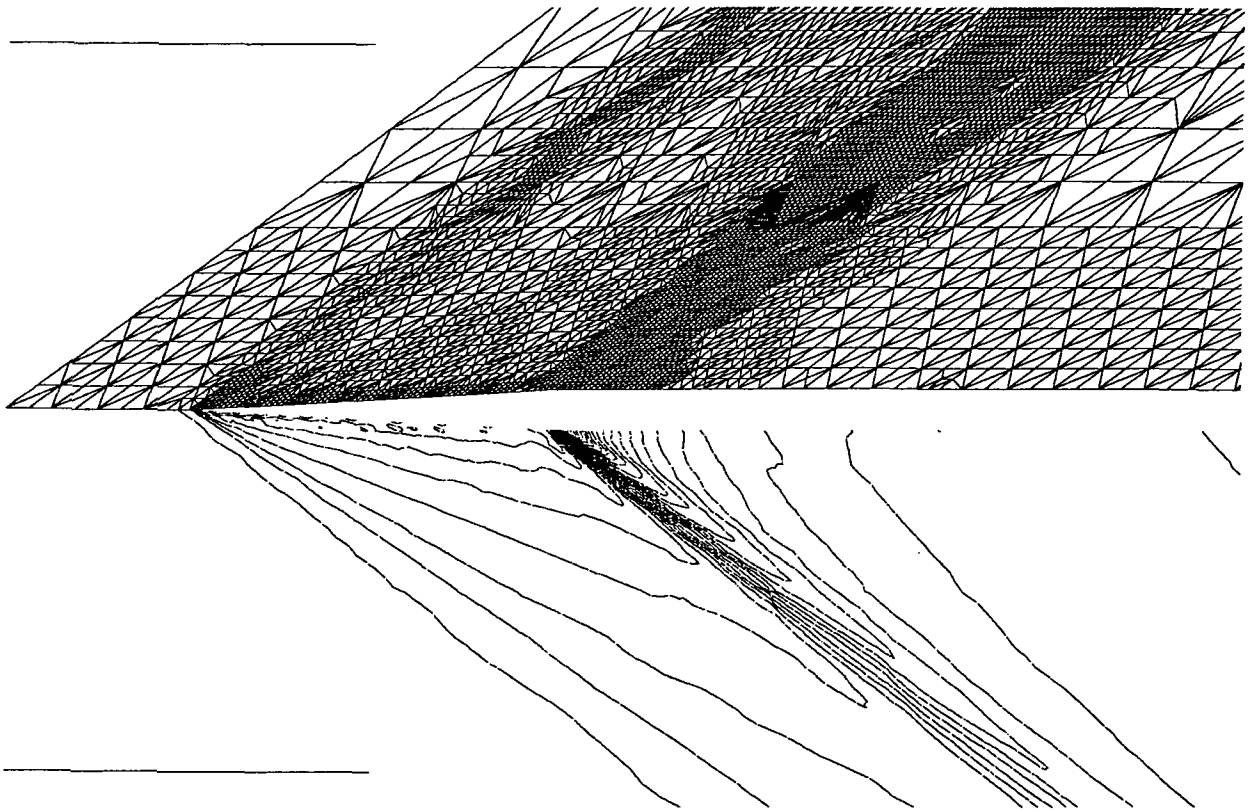

Figure 5: Close-up view of the final adapted mesh and pressure contours on the symmetry plane for the cone-cylinder, $M_\infty = 1.68$, $\alpha = 0.0°$.

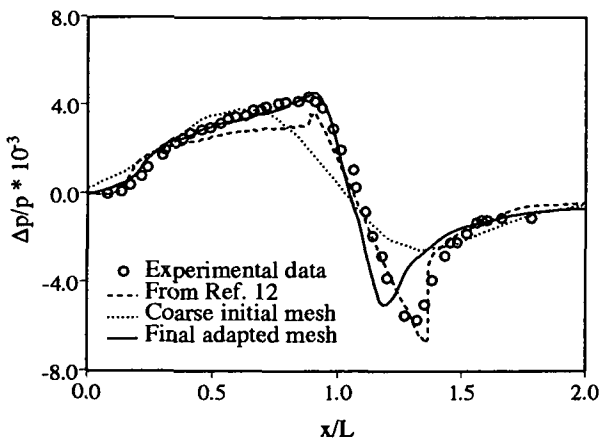

Figure 6: Pressure signature for the cone-cylinder, $M_\infty = 1.68$, $\alpha = 0.0°$, $h/L = 10.0$.

the likelihood of important flow features from being completely missed.

A total of four solution-adaptive steps were then performed. Innovative error indicators that include special shock finders have been used in earlier work[14] to adapt the computational mesh; however, using the absolute value of the pressure difference across an edge as a measure of the error worked remarkably well. This decision criterion was very effective in capturing flow gradients at the leading edge, in the upper surface expansion, and at the shocks. The residual was reduced by at least three orders on each intermediate mesh using FLOPLANE.

Table 2 presents the progression of grid sizes through the five adaption steps. The final adaption was prevented from refining edges that lay within a cylindrical region of radius 0.04 centered around the leading edge stretching from the symmetry plane to the outer spanwise boundary. The leading edge region was already adequately resolved since the pressure gradients are large and the adaption method refines this region first. New points were added along the surface shocks in the final refinement step in an attempt to accurately capture the shocks. The final mesh therefore has four levels of refinement near the leading edge but five levels along the shocks.

For the purposes of critically evaluating the adapted mesh and solution, FLOPLANE was also run on a uniformly fine mesh (224,354 points, 1,352,104 elements, and 1,598,508 edges) generated

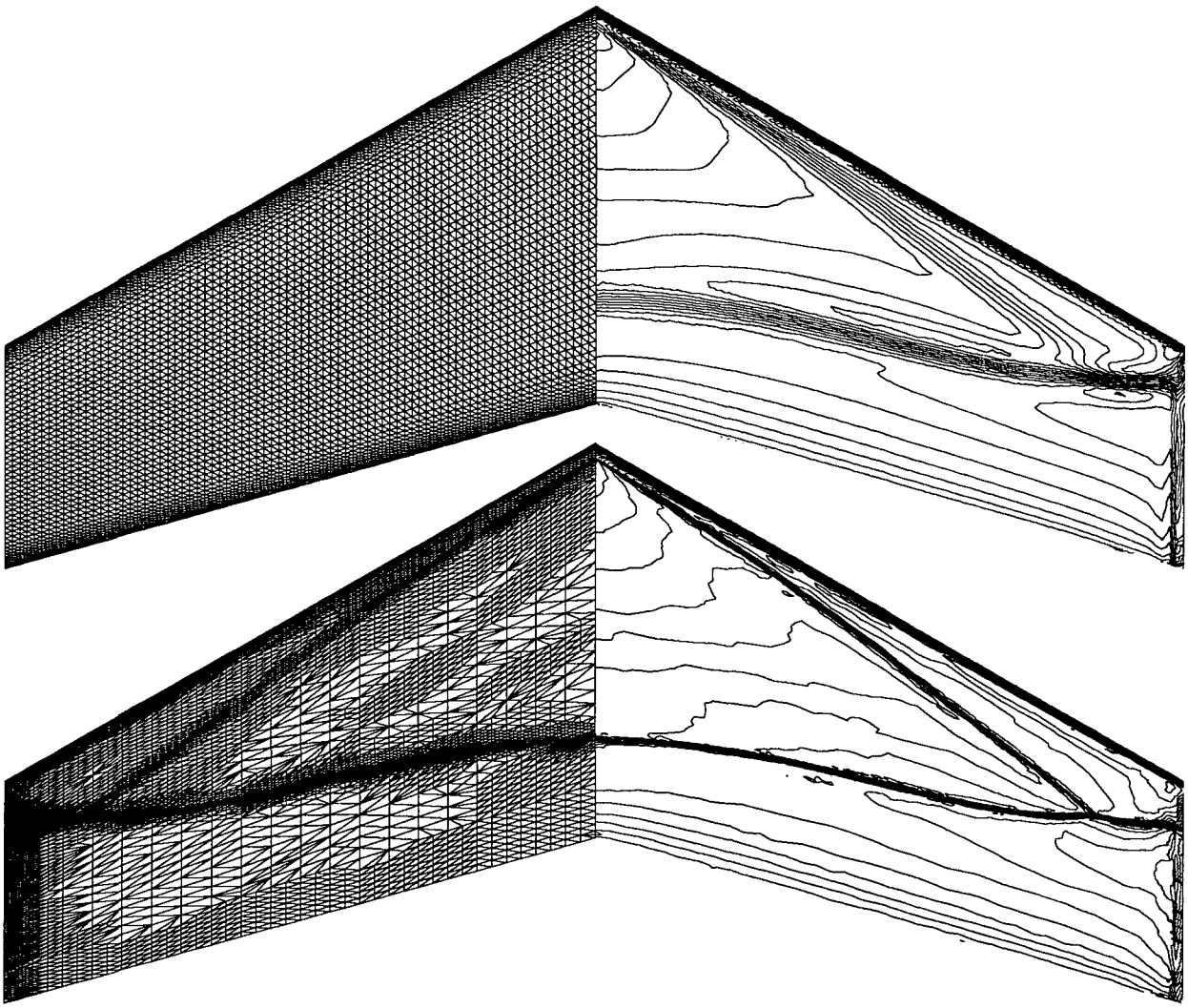

Figure 7: Finest MESHPLANE and final adapted meshes and corresponding pressure contours on the upper surface of the ONERA M6 wing, $M_\infty = 0.84$, $\alpha = 3.06°$.

Table 2: Grid sizes through the adaption steps

	Vertices	Elements	Edges
Initial mesh	34,202	153,706	194,657
Geom. ref.	40,036	185,232	232,610
1st adapt.	87,058	455,060	551,795
2nd adapt.	153,326	834,834	1,001,925
3rd adapt.	227,433	1,260,069	1,505,058
4th adapt.	325,901	1,830,957	2,176,617

by MESHPLANE.

Figure 7 shows the MESHPLANE and the final solution-adapted meshes along with the corresponding pressure contours on the upper surface of the wing. Note that the resolution is significantly improved along the shocks for the adapted mesh even though it has only 9802 surface points compared to 11,718 for the MESHPLANE mesh. It is obvious that the adapted mesh with fewer points has resulted in more distinct shocks.

During each refinement step, a previously-generated database of grid points defining the wing surface with very high resolution was interrogated to ensure that all new surface points lie on the wing. This was required because the regular edge-midpoint refinement scheme would have preserved the initial faceting of the wing surface.

Computed pressure coefficients on the final adapted mesh at four span locations are presented in Fig. 8. These results are compared to experimental data collected by Schmitt and Charpin.[13]

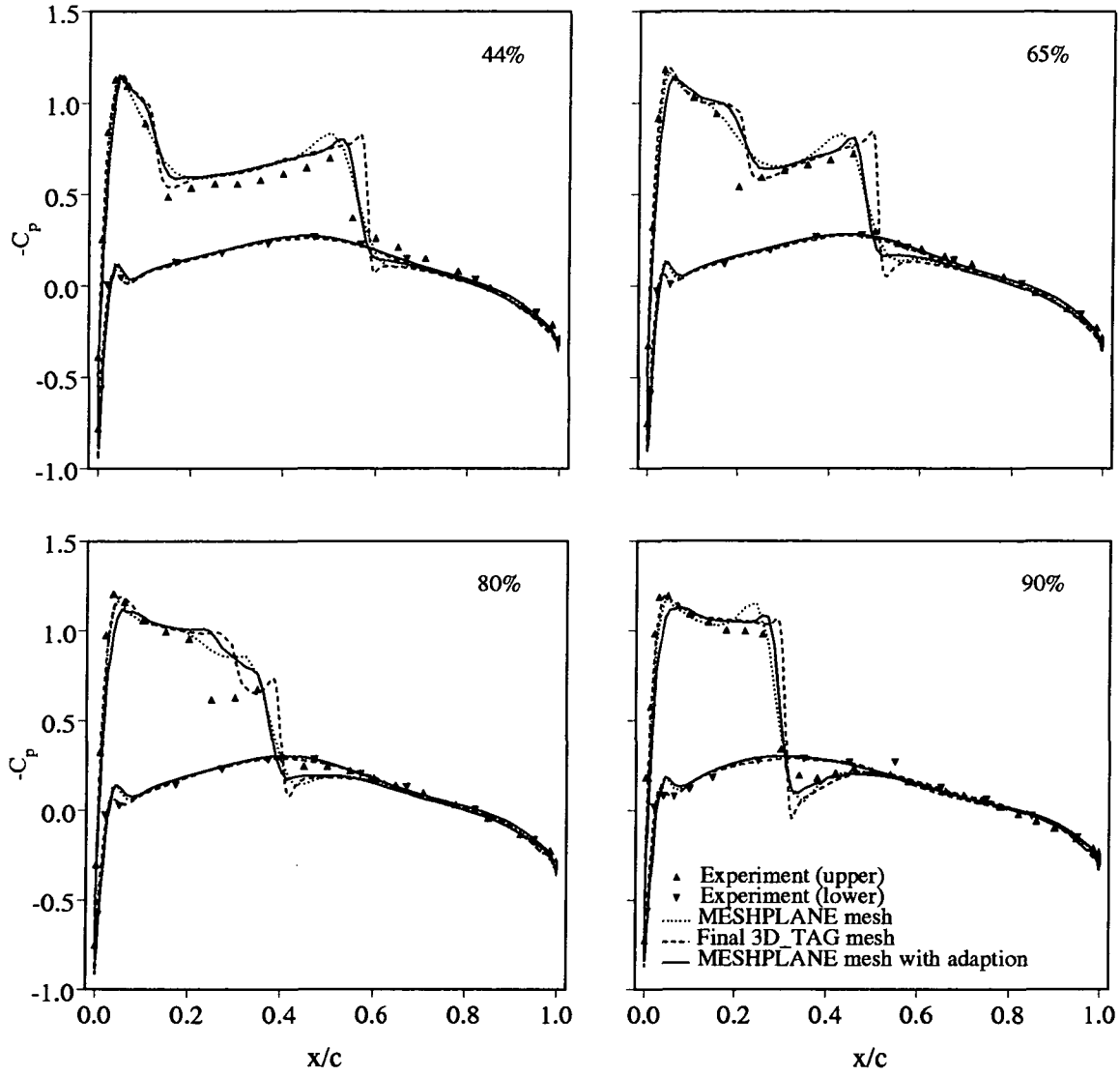

Figure 8: Comparison of surface pressure distributions at 44%-, 65%-, 80%-, and 90%-span stations for the ONERA M6 wing, $M_\infty = 0.84$, $\alpha = 3.06°$.

The experimental data is shown only as a reference, since the inviscid Euler solutions will not agree with the data. These results are also compared to results obtained on the globally fine mesh generated by MESHPLANE, and results obtained after one adaption of this mesh. Adapting the mesh from MESHPLANE would be the typical method for improving the solution. Fewer refinement levels should be necessary when starting from a uniformly fine mesh, which should reduce the chances of developing tetrahedra of poor quality when subdivided.

The solution obtained with the mesh adapted from the coarse structured grid shows better shock definition than the other computations and captures both shocks. It is well known that an accurate Euler solution will predict shocks that are stronger and aft of experiment, as is the case with these computations. It is not possible to determine whether this solution represents the most accurate Euler result of the three solutions shown, since the strength and location of the shocks for an accurate inviscid result are not known.

The results for the non-adapted mesh have less crisp shocks, and the forward shock at these stations is not adequately captured. The results of one adaption of the MESHPLANE grid more accurately captures the forward shock shown in the three inboard span stations, but the the shocks are not as well defined as the shocks obtained from the coarse structured grid. It would be expected that further

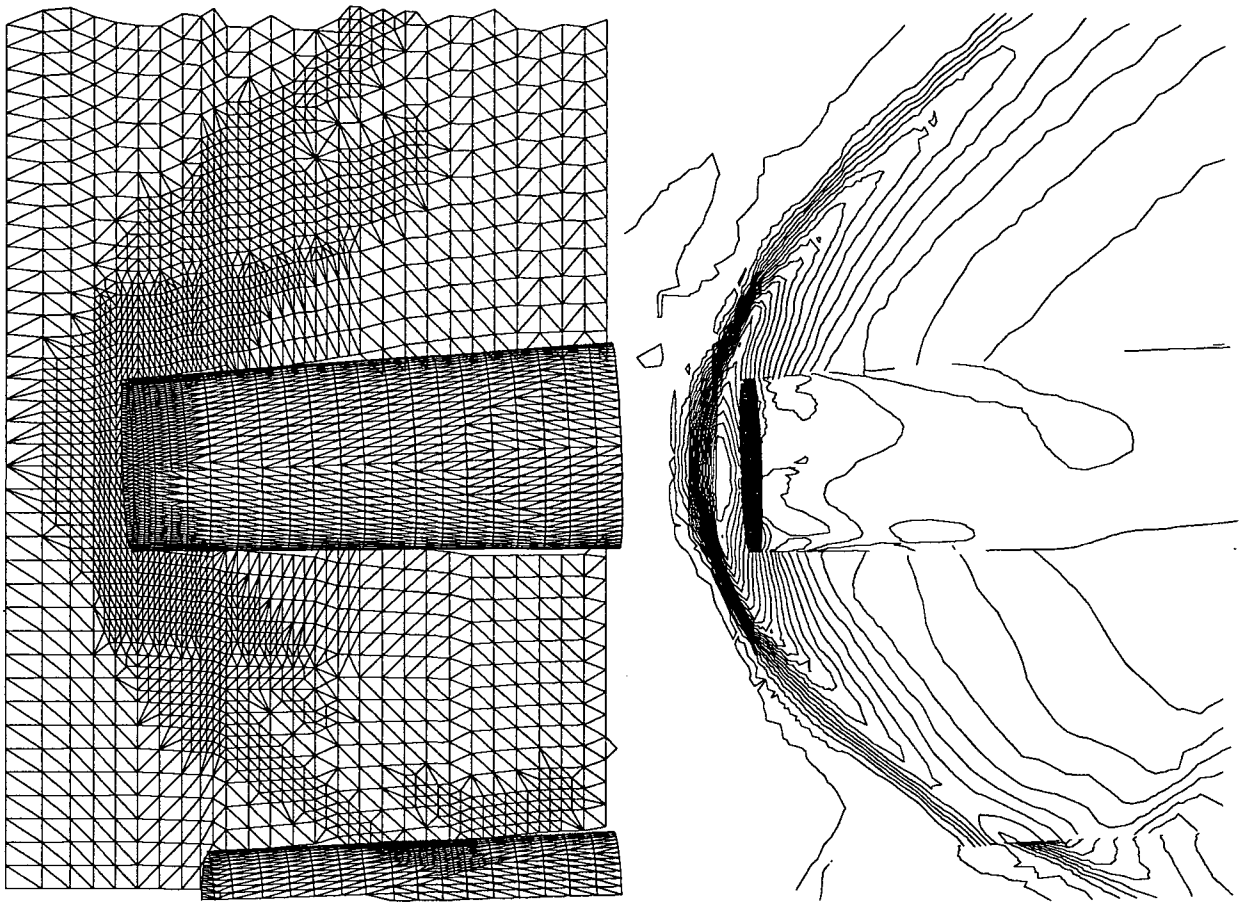

Figure 9: Close-up view of the final adapted mesh and pressure contours on the lower surface of the supersonic transport configuration.

grid refinement steps would lead to more sharply defined shocks.

The results for one adaption of the standard mesh and the non-adapted grids do correlate better with experiment, but this is due to the artificial viscosity in the numerical scheme mimicing the actual viscosity. The reduced cell size in the vicinity of the shocks associated with the adapted meshes, led to pre- and post- shock pressure fluctuations, which were damped by increasing the local dissipation parameter in FLOPLANE.

The final test problem is a complete supersonic transport configuration including nacelles. Only half the aircraft needs to be modeled because of symmetry. The outboard nacelle is plugged to simulate inlet unstart. This causes a bow shock to be formed upstream of the plugged nacelle at supersonic speeds. This shock impinges on the lower surface of the wing and also reflects off the inboard nacelle. Adaptive mesh refinement using the 3D_TAG code was performed in this region to accurately capture the shock and help understand more of the flow physics.

The initial MESHPLANE mesh consisted of 457,712 grid points and over 2.75 million tetrahedral elements. More than 40,000 iterations were required to produce a well-converged solution. One mesh adaption was then performed within a rectangular region enclosing the bow shock using pressure differences across edges as the error indicator. This increased the mesh size to 497,211 points and about 3 million tetrahedra.

The final mesh and pressure contours on the lower surface of the configuration in the vicinity of the nacelles are shown in Fig. 9. Only triangles with visible centroids are drawn in order to approximately hide triangles behind the nacelles. In the initial mesh, streamwise mesh density was doubled in a rectangular region of the wing surface near the inlet, but the bow shock was upstream of this region. 3D_TAG refined much of the rectangular region and also elements ahead of it, where the pressure differ-

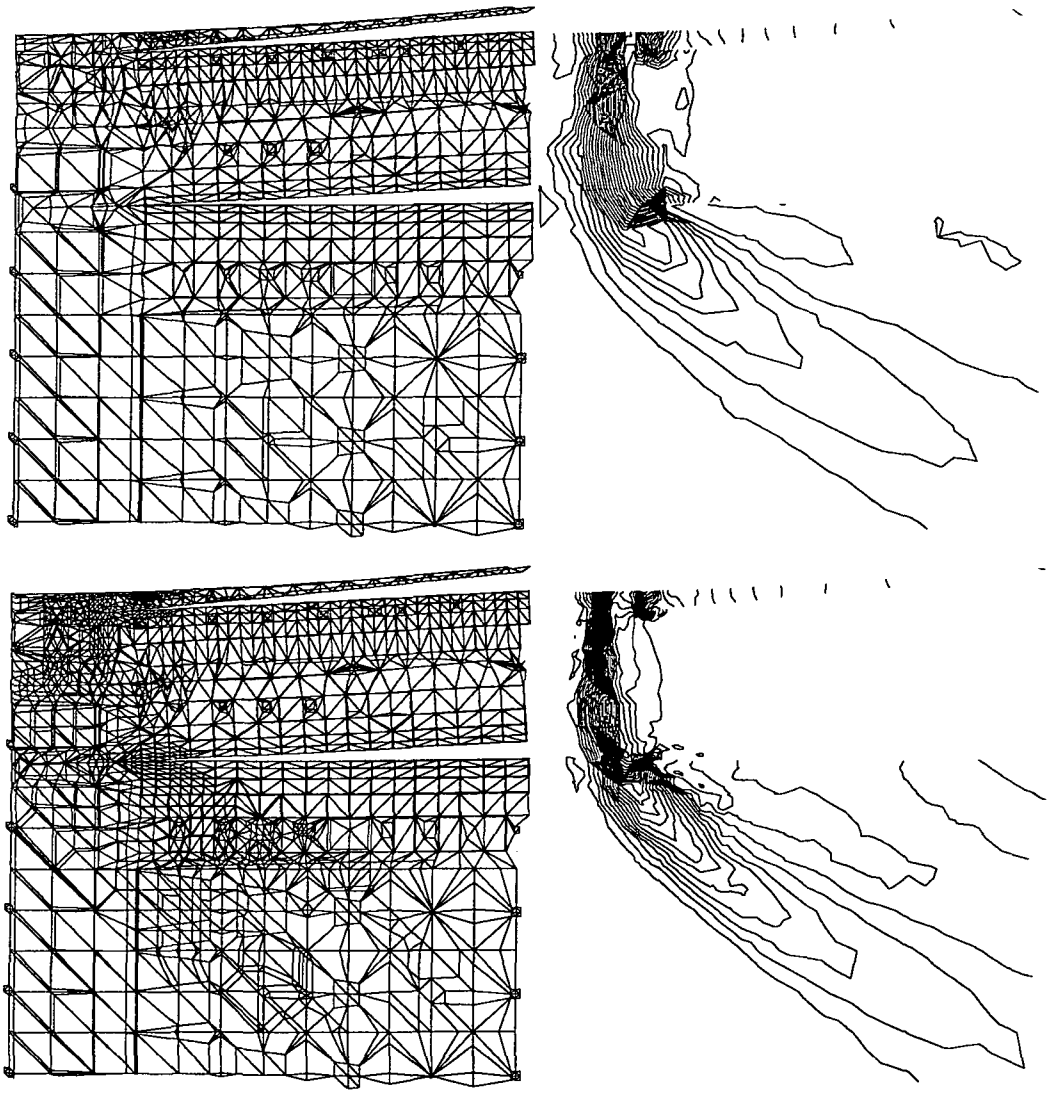

Figure 10: Pressure contours on a planar slice through the axis of the plugged nacelle before and after mesh refinement.

ences along edges were large. There is refinement near the leading edge of the plugged inlet and where the bow shock strikes the inboard nacelle. The inlet of the inboard nacelle was not refined because air flows supersonically through it with a relatively small pressure gradient.

Meshes and pressure contours are shown on a vertical cutting plane aligned with the axis of the plugged nacelle for the initial and final meshes in Fig. 10. The slices are composed of triangles and quadrilaterals. Pressure values are obtained by linear interpolation from the node-based solutions on the tetrahedral meshes. Refinement follows the strongest portion of the bow shock and is swept in a fashion similar to that observed on the surface. The width of the shock is roughly cut in half. Pressure differences are very high at the lip of the inlet, both inside and out, and in the gap between the inlet leading edge and the lower wing surface.

Figure 11 presents a qualitative comparison of the pressure ratio along the axis forward of the plugged nacelle on the initial and refined meshes. As noted above for Fig. 10, the shock on the refined mesh is half as wide as on the initial mesh. Pre- and post-shock oscillations are also confined to a narrower region on the refined mesh. The pressure ratio ahead of the shock is the same for both meshes, but the predicted change in pressure ratio is 4.5% higher for the refined mesh.

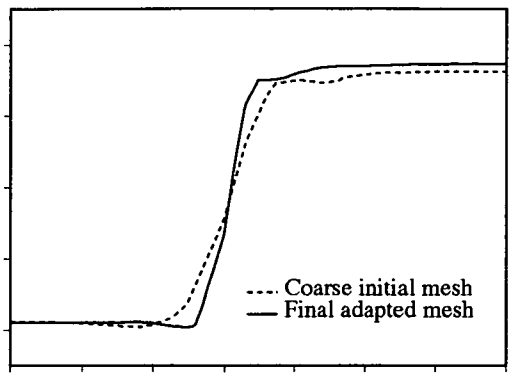

Figure 11: Variation of the pressure ratio along the axis of the plugged nacelle.

SUMMARY

The tetrahedral mesh adaption scheme was successfully coupled to the AIRPLANE code. The near-field sonic boom pressure signature on a cone-cylinder was improved by adapting the mesh. The finite-rise bow shock and maximum overpressure were more accurately predicted. The sampling distance was increased for the adapted grid solution, which is important because typical aircraft require a sampling distance of approximately one semispan to capture three-dimensional effects.

The solutions for the ONERA M6 wing with grid refinement based on pressure gradient more accurately captured the lambda shock on the upper surface. The adapted meshes captured a forward shock which was not seen in the solution with a uniform mesh; the shocks were more sharply defined. Increased local dissipation was required to damp pre- and post-shock pressure fluctuations on the adapted mesh cases.

3D_TAG was successfully used to more sharply resolve the bow shock of an unstarted inlet on a supersonic transport. Results presented in this report demonstrate that 3D_TAG and AIRPLANE have been successfully coupled and applied to realistic flow problems.

REFERENCES

[1]Biswas, R., and Strawn, R. C., "A New Procedure for Dynamic Adaption of Three-Dimensional Unstructured Grids," *Applied Numerical Mathematics*, Vol. 13, No. 6, 1994, pp. 437–452.

[2]Jameson, A., Baker, T. J., and Weatherill, N. P., "Calculation of Inviscid Transonic Flow Over a Complete Aircraft," AIAA Paper 86-0103, AIAA 24th Aerospace Sciences Meeting, Reno, NV, Jan. 1986.

[3]Jameson, A., and Baker, T. J., "Improvements to the Aircraft Euler Method," AIAA Paper 87-0452, AIAA 25th Aerospace Sciences Meeting, Reno, NV, Jan. 1987.

[4]Barth, T. J.,"A 3-D Upwind Euler Solver for Unstructured Meshes," AIAA Paper 91-1548, AIAA 10th Computational Fluid Dynamics Conference, Honolulu, HI, Jun. 1991.

[5]Strawn, R. C., Biswas, R., and Garceau, M., "Unstructured Adaptive Mesh Computations of Rotorcraft High-Speed Impulsive Noise," *Journal of Aircraft*, Vol. 32, No. 4, 1995, pp. 754–760.

[6]Duque, E. P. N., Biswas, R., and Strawn, R. C., "A Solution Adaptive Structured/Unstructured Overset Grid Flow Solver with Applications to Helicopter Rotor Flows," AIAA Paper 95-1766, AIAA 13th Applied Aerodynamics Conference, San Diego, CA, Jun. 1995.

[7]Baker, T. J., "Generation of Tetrahedral Meshes Around Complete Aircraft," 2nd International Conference on Numerical Grid Generation in Computational Fluid Dynamics, NASA and Airforce Office of Scientific Research, Dec. 1988.

[8]Baker, T. J., "Automatic Mesh Generation for Complex Three-Dimensional Regions Using a Constrained Delaunay Triangulation," *Engineering with Computers*, Vol. 5, Nos. 3 and 4, 1989, pp. 161–175.

[9]Jameson, A., Cliff, S. E., Thomas, S. D., Baker, T. J., and Cheng, W-S., "Supersonic Transport Design on the IBM Parallel System SP2," NASA Computational Aerosciences Workshop, Moffett Field, CA, Mar. 1995.

[10]Biswas, R., and Strawn, R. C., "Mesh Quality Control for Multiply-Refined Tetrahedral Grids," *Applied Numerical Mathematics*, to appear.

[11]Thomas, C. L., "Extrapolation of Sonic Boom Pressure Signatures by the Waveform Parameter Method," NASA TN D-6832, Jun. 1972.

[12]Cliff, S. E., and Thomas, S. D., "Euler/Experiment Correlations of Sonic Boom Pressure Signatures," *Journal of Aircraft*, Vol. 30, No. 5, 1993, pp. 669–675.

[13]Schmitt, V., and Charpin, F., "Pressure Distributions on the ONERA-M6-Wing at Transonic Mach Numbers," AGARD Report AR-138, 1979.

[14]Melton, J. E., Thomas, S. D., and Cappuccio, G., "Unstructured Euler Flow Solutions using Hexahedral Cell Refinement," AIAA Paper 91-0637, AIAA 29th Aerospace Sciences Meeting, Reno, NV, Jan. 1991.

RIACS
Mail Stop T041-5
NASA Ames Research Center
Moffett Field, CA 94035